Bull. Chem. Soc. Jpn., 70, 1225—1238 (1997)

Accounts

Spectroscopy and Photophysics of O_2 in the Neighborhood of the Dissociation Limit in Rare Gas Solids

Seiichiro Koda* and Hideo Kajihara

Department of Chemical System Engineering, School of Engineering, The University of Tokyo, Hongo 7-3-1, Bunkyo-ku, Tokyo 113

(Received January 6, 1997)

The energy levels, potentials and relaxation mechanism of O_2 doped in rare gas (Ar, Kr) and N_2 solids in the neighborhood of the dissociation limit have been studied by means of absorption and emission spectroscopy. The environmental effects of the solids on the energy level shift are not large, but the cage effect is important in considering the relaxation mechanism following the laser irradiation. The efficient cross-relaxation among nested Herzberg states and specific energy transfer dependent on the energy gap between relevant levels, in particular from A′ state to c state, have been found. Due to the very slow vibrational relaxation, vibrationally excited O_2 molecules have been accumulated to a high concentration in the solid. Based on the B–X transition energy values from the vibrationally excited O_2 molecules, the B state potential curve has been determined. This shows that the cage effect retards the atomic dissociation in the B state.

The oxygen molecule has three metastable states ($A(^3\Sigma_u^+)$, $A'(^3\Delta_u)$, $c(^1\Sigma_u^-)$) named Herzberg states just below the dissociation limit, which is 41256.6±3.8 cm^{-1} ($D_0(X)$) or 42044.2±3.8 cm^{-1} ($D_e(X)$) in the gas phase. The spectroscopy of Herzberg bands, although they are extremely weak, has been extensively, though not completely, carried out in the gas phase since the first observation by Herzberg.[1—5] Very weak absorption lines near the dissociation limit have been only very recently measured by the technique of cavity ring-down spectroscopy to find the high vibrational levels, $A(v=12)$, $A'(v=12,13)$ and $c(v=17,18)$ levels, together with a large number of unidentified lines.[6] The mechanism of absorption intensity augmentation under the pressurized gases has been also studied.[7] On the other hand, the lowest allowed electronic state is B state, which is predissociatively correlated with the first dissociation limit to yield $O(^3P)+O(^3P)$. The spectroscopy of the Schumann–Runge band corresponding to the above B–X transition is abundant in the gas phase.

Compared to the rather extensive studies in the gas phase, there are only a few publications dealing with the spectroscopic and photophysical behavior of Herzberg as well as Schumann–Runge bands in solids. Solid state studies address many intriguing problems. In the gas phase, O_2 can be efficiently dissociated through the Schumann–Runge absorption. In solids, however, the dissociation is extremely inefficient due to the so-called cage effect. The effect of surrounding solids on the electronic and vibrational relaxation of the center molecule is quite important. The present authors have aimed at understanding the total picture of O_2 behavior excited in rare gas and N_2 solids with KrF (at 248 nm=5.0 eV) and ArF (at 193 nm = 6.4 eV) excimer lasers. The objective of this account is to describe the present day understanding of solid-state spectroscopy, potentials and photophysical behavior of O_2 excited near the dissociation limit.

1. Properties of Solids. Some important properties of the rare gas and N_2 solids are tabulated in Table 1. They have the fcc structure. The individual properties are not far apart from each other, though the compressibility of Ne is exceptionally large. This softness of the Ne solid may contribute interesting features to its cage effect. However, its relatively low triple point makes the extensive work using Ne as the host solid somewhat difficult. Xe solid sometimes behaves differently from other rare gas solids due to its large polarizability, which is the probable cause of the relatively easy excimer formation between the oxygen atoms and Xe lattice atoms, which will be discussed later.[8] The properties of N_2 solid are similar to those of Ar solid.

The Debye frequency is similar for all these rare gas and N_2 solids. This frequency is the maximum frequency of the elastic continuum according to Debye theory, where the relative density of the eigenfrequencies in the spectrum of the molecular lattice is essentially identical with the distribution of the ordinary elastic eigenfrequencies of vibration of

Table 1. Properties of Host Molecules and Solids[a)]

	Ne	Ar	Kr	Xe	N_2
Atomic diameter/nm	0.30	0.38	0.42	0.46	0.434 0.339
Polarizability/10^{-24} cm^3	0.395	1.64	2.48	4.04	1.76[c)]
Space group	fcc[b)]	fcc	fcc	fcc	α-N_2[d)]
Triple point T/K	24.6	83.8	115.8	161.4	63.15
P/bar	0.43	0.69	0.73	0.81	0.13
Density (at 15 K)/10^{-2} mol cm^{-3}	7.44	4.46	3.68	2.88	3.66
Lattice constant (at 15 K)/nm	0.447	0.531	0.565	0.613	0.566
Compressibility (T=constant)/10^{-10} Pa^{-1}	8.92	3.74	2.90	2.80	4.64
Thermal Conductivity (at 20 K)/W m^{-1} K^{-1}	0.4	1.3	1.2	2	0.4
Debye frequency (at 0 K)/cm^{-1}	75	93	72	64	69

a) Ref. 39. b) Face centered cubic lattice. c) Mean polarizability. d) The stable phase of N_2 at lower than 35.61 K is α-N_2. Molecular axes are fixed to the lattice (fcc).

a continuous elastic medium. This frequency may be taken as an index of a phonon quantum when considering the energy flow probability from the doped molecules to the lattice modes.

The host solids described in this account are mainly Ar, Kr, and N_2. These three solids exhibit similar environmental effects to the doped O_2, at least qualitatively. In some cases, Xe and H_2 as solids will be explained.

2. Free-Standing Crystal. In the study of the present authors, O_2 is doped in free-standing crystals according to the method of Schwentner et al.[9] in place of matrices which are usually employed in the works of other researchers. Thus it is worthwhile to briefly describe the preparation procedure of the free-standing crystal, which is of a relatively large volume containing grains of several tenths of mm in size according to X-ray analysis.[10]

The cryostat system that we used for preparation of the free-standing crystal is shown in Fig. 1. A typical procedure for the preparation of O_2-doped Ar is as follows. A bottomless glass cup of $10\times10\times20$ mm^3 equipped with a gas-inlet tube is pressed against the head of a copper cryotip, which is kept at 16 K (by a closed-cycle refrigerator) in a vacuum chamber. The crystal is grown in the cup for 20 min by deposition of a mixture of O_2 and Ar, which has been prepared beforehand, at a total pressure of 150—350 Torr (1 Torr = 133 Pa). When the deposition is completed, the glass cup is removed upward and a free-standing crystal remains on the head of the cryotip. In the study of photophysics, the whole crystal is irradiated by appropriate lasers, and the emission or absorption measurements are performed along the perpendicular direction to the irradiation laser beam.

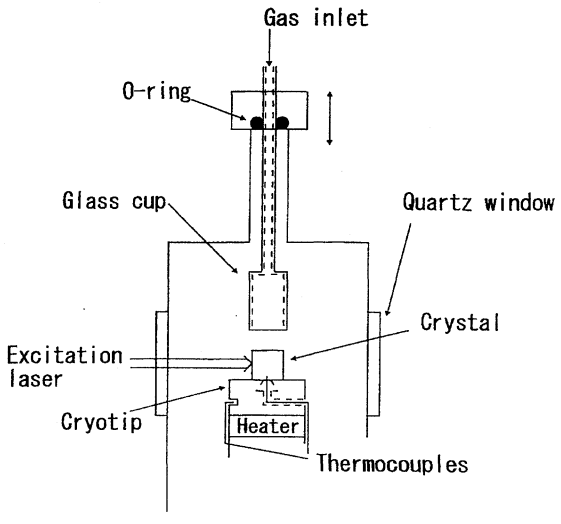

Fig. 1. The apparatus for preparation of free-standing crystals.

The great advantage of the free-standing crystal is that it offers a long absorption path length and a smaller scattering of the irradiation laser, particularly in the shorter wavelength region such as the UV region. The list of typical studies which have been performed using the free-standing crystal is shown in Table 2. The usage of the free-standing crystal has been limited to several research groups, probably because it is sometimes difficult to obtain well isolated guest molecules in free-standing crystals. The environmental difference between the free-standing crystal and matrices is not apparent in most cases treated in the present account. Thus the "solid" in the present account means matrices and/or free standing crystals without distinction.

Energy Levels of Herzberg States in the Gas Phase

The gas-phase potential curves relevant to the present account are illustrated in Fig. 2, which has been reproduced from the review work of Krupenie.[2] Absorptions to the three states which are correlating with the dissociation limit to yield two O(^{3}P) atoms are collectively known as the Herzberg transitions. The A–X band is the Herzberg I system, the c–X band is Herzberg II, and the A′–X band is Herzberg III. The transition moments are, small as they are, derived from interactions with states lying above the dissociation limit and these interactions are not localized. Although the metastability impeded the spectroscopic study, Slanger and Cosby[11] summarized a considerable amount of spectroscopic information on the Herzberg states and also on the other two low lying metastable states (a, b) in 1988. As reproduced from their article, the vibrational level energies of the relevant states are shown in Fig. 3, which may be useful as a reference for the later discussions on the vibronic relaxation

Table 2. List of the Studies of Free-Standing Crystal

Group	Objective	Crystal	Method	Ref.
Schwentner's group	Stimulated emission from excited rare gas	Ar, Kr, Xe	Emission	9, 10
	Vibrational relaxation of N_2	Kr and Xe	LIF, Raman	47
Apkarian's group	Production of excimer	Xe	LIF	8
	Photo-stationary state of O_2	Ar and Kr	LIF	41
	Diffusion of O atom	Kr and Xe	LIF	20, 26, 27
	Segregation of N_2O	Ar and Xe	FT-IR	48
The present group	Multi-photon excitation of N_2	N_2	LIF	49
	Relaxation of excited O_2	Ar and N_2	LIF	16, 17
	Accumulation of vibrationally excited O_2	Ar	UV-Absorption	30
	Production of excimer	Xe	LIF	50

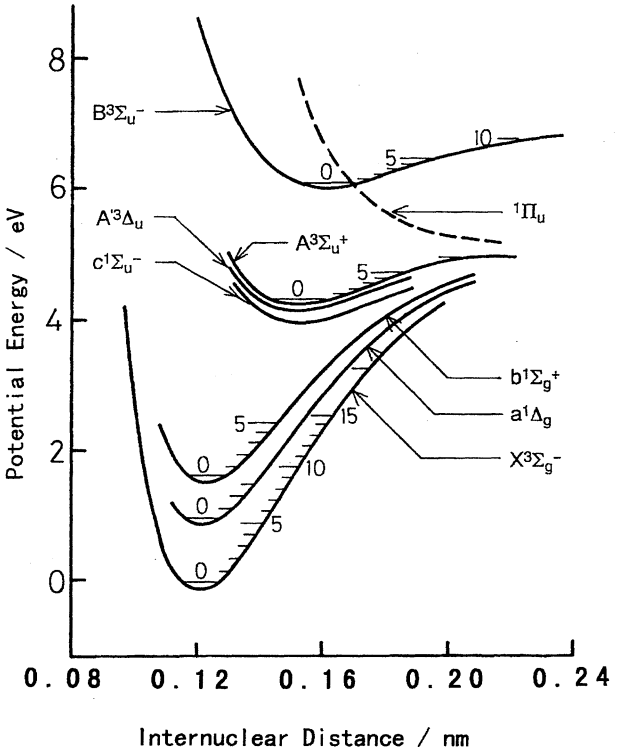

Fig. 2. Potential energy curves of O_2. The original data are from Ref. 2.

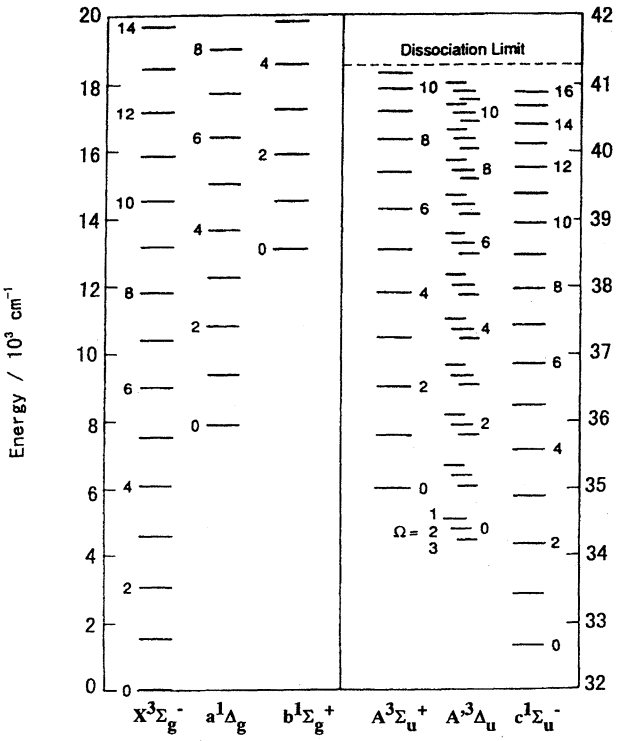

Fig. 3. The vibrational energy levels of relevant states of O_2. The original data are from Ref. 11.

mechanism in solids. For the zero of energy, the origin (T_0) of the $^3\Sigma_g^-$ Hamiltonian of Zare et al.[12] that describes the $O_2(X)$ state is adopted. In this formation, the lowest existing level of the X state, the $J=0$, $N=1$, F_3 rotational level of $v=0$, lies 0.2459 cm^{-1} above the origin. The A and A′ states are similar, and different from the c state. The obvious difference is that the A and A′ states are both triplets, with an energy separation of 625 cm^{-1} at the equilibrium bond length, whereas the c state is a singlet state and lies 1715 cm^{-1} below the A′ state. Another important thing to notice is that the A′ state has three almost equally spaced subcomponents ($\Omega=3$, 2, and 1) separated by ca. 150 cm^{-1}. Herzberg's assignment labeled the lowest member of each triplet as $\Omega=1$.[1] The order of Ω subcomponents has been controversial, and it is currently accepted that the A′($^3\Delta_u$) state is an inverted spin-orbit multiplet,[4] as numbered in Fig. 3. We will adopt this assignment in this account. However, a very recent study of the O_2-doped D_2[13] matrix has strongly suggested that the state is a normal triplet even in the gas phase, in agreement with Herzberg. Whether the multiplet is normal or inverted is open to further investigation.

The B state potential curve is also drawn in Fig. 2 together with that of one repulsive state $^1\Pi_u$ as a representative of the repulsive states. The repulsive states which are responsible for the predissociation in the gas phase are $^3\Pi_u$, $^1\Pi_u$, $^5\Pi_u$, and $^3\Sigma_u^+$, among which the $^5\Pi_u$ predominantly contributes to the predissociation. Their estimated potential curves are found in the literature.[14]

Energy Levels of Herzberg States in Solids

The energy levels are located according to the spectroscopic measurements of relevant absorption and emission transitions. Essential works for the purpose are shown in Table 3 as a reference list, where the transitions relevant to the lower a and b states are also included.

1. A′←X Absorption and A′ State Levels. Goodman and Brus[15] obtained the 290—240 nm absorption of O_2 in solids for the first time. The spectra are most sharp in N_2 matrix and detailed studies have been performed only for those in N_2. Excitation spectra in solid N_2 have been also observed in the Herzberg region by using highly monochromatic dye laser light and monitoring the A′→X and also c→a emissions.[16] The example of A′←X excitation spectrum observed with monitoring different emission lines is shown in Fig. 4. The sharp lines observed at 14.9 K are assigned as zero-phonon lines of Ω components of A′ state. It is not evident from these spectra or subsequent ones which component of the A′ state radiates. Slanger and Cosby[11] presumed that at these low temperatures only the $\Omega = 3$ levels are populated. In the gas phase, A′ state radiates predominantly to a($^1\Delta_g$) in the Chamberlain band. However, the spin forbidden A′($v = 3$)→a emission has never been reported in matrices, and it is likely that, in the cold environment, the A′→X emission is much stronger. The middle member of the triplet undergoes an interesting change of shape as a function of v and also of isotope (not shown here). Goodman and Brus[15] have interpreted this phenomenon as a progression of perturbations, which causes intensity borrowing, level shift and lifetime broadening. As the perturbing state, they recommended $A^3\Sigma_u^+$. Indeed, v levels of the A′ state are almost degenerate with $v-1$ levels of the A state in the gas phase as shown in Fig. 3, with A lying below A′ for low v numbers and above A′ for high v numbers. The sharp zero phonon lines in the excitation spectra are also reported in solid D_2.[13]

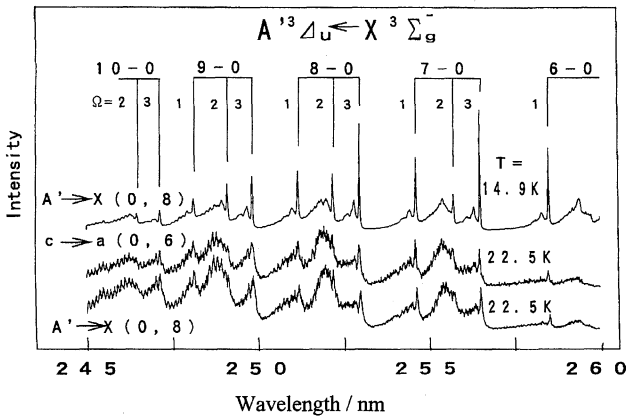

Fig. 4. Excitation spectra (A′←X) of O_2 doped in N_2 obtained by monitoring different emissions shown in the figure. The original data are from Ref. 16.

2. A′→X Emission and X State Levels. In most cases, the energy levels of O_2 Herzberg and ground states have been obtained from emission spectroscopy.[15] Resonant or dissociative excitation of O_2 in UV region above 5 eV produces vibrationally relaxed emission over the A′($^3\Delta_u$)–X transition. The A′ state is nested amid the A($^3\Sigma_u^+$) and the c($^1\Sigma_u^-$) potentials. The A′ state of O_2 transfers its population to the c state: the A′→X emission subsides, and is replaced by the c→a emission in some cases. The vibrational resonance required in this process is isotopically sensitive, such that the $^{16\text{-}18}O_2$ c→a emission dominates even when natural O_2 is adopted.

The spectrum of the long lived emissions (t = ca. 80 μs) observed in O_2-doped Ar solid irradiated by 193 nm ArF excimer laser light is shown in Fig. 5,[17] which is attributed to the A′ ($\Omega = 3$, $v' = 0$)→X (v'') progression by comparing the band positions with those reported previously[18,19] and also on the basis of the Franck–Condon envelope. The c→a emissions from the $v' = 2,1,0$ levels for $^{16\text{-}18}O_2$ were also observed with considerable intensities in spite of the low natural abundance (0.2%) of the ^{18}O isotope as mentioned above.

The line positions of the A′–X transition measured by various researchers[17,18] are tabulated in Table 4, together with corresponding data in the gas phase. The table shows that the stabilization of A′ state (relative to X state) from the gas phase is around 100 cm^{-1}, provided that the X state energies are not affected by the surrounding solids.

3. c→a Emission and c State Levels. Along with the long lived emissions, existence of short-lived emissions (t=80 ns) was recognized under the irradiation by 193 nm light. From the comparison of the peak positions with the corresponding peak positions in the gas phase and Franck–Condon intensity distribution calculations, the emission was assigned as c ($v' = 5$)→a transitions. The peak positions are tabulated in Table 5.[17] They deviate only slightly to the red side from the gas phase values. For example, the difference between the solid and gas-phase peak position for the 5–0 transition of the c→a emission is 49 cm^{-1}, in comparison with that of 108 cm^{-1} for the 0–5 transition of the A′→X transition. The matrix shifts for the c and a states are considered to be small as in the case of A′ and X states. Some

Table 3. List of the Transitions of $^{16}O_2$ Studied in Low-Temperature Solids

	Ne	Ar	Kr	Xe	N_2
A′-X	—	Ref. 15, 17, 22, 51	Ref. 22, 51	—	Ref. 15, 16, 51
c-a	—	Ref. 17	—	Ref. 22	Ref. 16
b-X	—	Ref. 31	Ref. 20	—	—
a-X	—	Ref. 52	—	—	—
B-X	Ref. 32, 35	Ref. 30, 32, 34—36, 44	Ref. 32, 35, 36, 44	Ref. 32, 35, 36	Ref. 32, 34

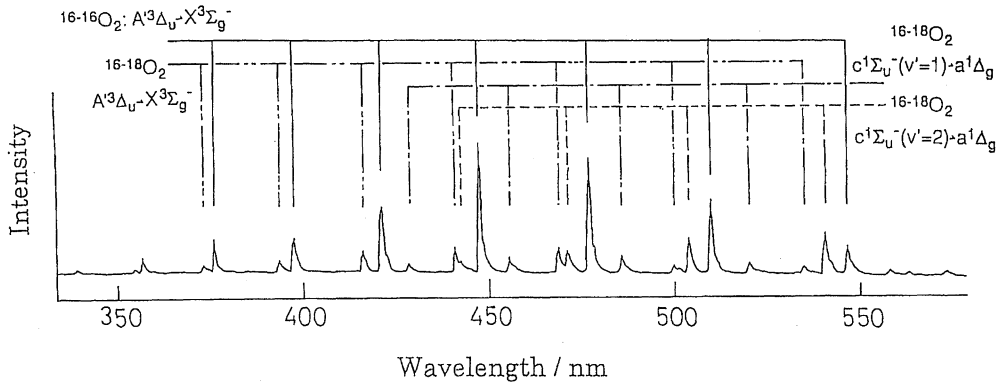

Fig. 5. Emission spectra with long lifetimes from O_2-doped Ar crystal at 193 nm. O_2/Ar = 1/700, Boxcar gate = 0—500 μs. The original data are from Ref. 17.

Table 4. Energy Difference in Emission Lines for the A′→X Transitions

Band (v', v'')	Gas[a] ν/cm^{-1}	in Ar[b] ν/cm^{-1}	in Ar[c] ν/cm^{-1}	ΔE[d] ν/cm^{-1}
(0, 3)	29636	29528	29512	−108
(0, 4)	28150	28041	28036	−109
(0, 5)	26687	26579	26584	−108
(0, 6)	25246	25160	25152	−87
(0, 7)	23829	23745	23741	−83
(0, 8)	22434	22358	22346	−76
(0, 9)	21061	20981	20981	−80
(0, 10)	19711	19644	19634	−67
(0, 11)	18384	18321	18311	−63
(0, 12)	17080	17019	17012	−61
(0, 14)	14540	14487	—	−53
(0, 15)	13249	13304	—	−55

a) Ref. 11. b) Ref. 17. c) Ref. 18. d) Energy (Ar, Ref. 17) − energy (gas phase).

Table 5. Energy Difference in Emission Lines for the c→a Transitions

Band (v', v'')	Gas[a] ν/cm^{-1}	in Ar[b] ν/cm^{-1}	ΔE[d] ν/cm^{-1}
(5, 0)	28326	28277	−49
(5, 1)	26842	26816	−26
(5, 2)	25384	25354	−30
(5, 3)	23953	23943	−11
(5, 4)	22548	22541	−7
(5, 5)	21169	21175	+5
(5, 6)	19817	19815	−2
(5, 7)	18492	18490	−2
(5, 8)	17195	—	—
(5, 9)	15925	15935	+11
(5, 10)	14683	14685	+3

a) Ref. 11. b) Ref. 17. c) Energy (in Ar) − energy (gas phase).

peak positions of c→a emissions ($v' = 2,1,0$) for $^{16\text{-}18}O_2$ in Ar and Kr are already given by Rossetti and Brus.[18]

In conclusion, the energy levels of Herzberg states in solids are in near coincidence (within 100 cm^{-1}) with those in the gas phase. The obtained spectroscopic constants for the relevant states together with the gas phase values are summarized in Table 6. The B state values which will be discussed later are also included.

Vibronic Relaxation Mechanism

As already stated, resonant or dissociative excitation of O_2 in UV region above 5 eV produces vibrationally relaxed emission over the A′–X transition. The emission spectrum has been already shown in Fig. 5. The c→a emissions of $^{16\text{-}18}O_2$[18] and b→X emissions are also observed in Ar and Kr matrices.[20]

1. Recombinant and Absorption-Induced A′→X Emission. In the case of 193 nm ArF excimer laser irradiation, intense recombinant emission is observed, indicating that the molecule is efficiently excited by the radiation, despite the fact that the excitation wavelength falls between vibronic resonances in the B–X Schumann–Runge band. While the B state is known to be predissociative via the repulsive curves, mainly $^5\Pi_u$[14,21] in the gas phase, it does not lead to efficient cage exit of O atoms in the solid. Although permanent dissociation occurs upon 193 nm excitation of O_2, as verified by observing LIF from O centers, this constitutes only ca. 1% of the molecules according to Danylichev and Apkarian,[20] as verified by their near constancy of LIF intensity from the molecular species all through the irradiation. That only O_2 molecules at defect sites undergo dissociation is a possibility. The excitation leads to the predissociative B state, and the subsequent molecular fluorescence is due to geminate recombination on the various surfaces that correlate with the dissociation limit to yield two O(^{3}P) atoms.

The problem to be solved is, thus, the nascent distribution just after the irradiation. After being repelled at the cage wall, the dissociated two O(^{3}P) atoms are recombined in the same cage to form the $A^3\Sigma_u^+$, $A'^3\Delta_u$ or $c^1\Sigma_u^-$ states. It is difficult to precisely estimate the nascent population of individual states, but it is certain that some part goes to the c state. In the gas phase, the emissions from the c state are observed through the recombination of O(^{3}P) atoms.[3] The qualitative agreement of emissions among different excitation wavelengths (193, 248 nm and others) would imply that the partitioning of population between the nested A, A′, and c potentials occurs deep inside the bound potentials, and has little memory of the mixing between states at the stretched

Table 6. Molecular Constants of Electronic States of O_2 in Low Temperature Solids (in cm^{-1} Unit)

	in Ne	in Ar	in Kr	in Xe	in N_2	Gas phase
X state						
T_e		0	0	0	0	0
ω_e	—	1581.07±1.10,[b] 1569.5[c]	1581.5[c]	—	1577.4[c]	1580.19[k]
ω_{exe}	—	12.70±0.34,[b] 11.16[c]	11.88[c]	—	11.79[c]	11.98[k]
ω_{eye}	—	0.07±0.03[b]	10^{-4} [c]	—	0.022[c]	0.05[k]
a state						
T_e	—	7923.5[b]	—	—	—	7918.1[k]
ω_e	—	1512.0[b]	—	1500.6[e]	1507.5[g]	1509.3[k]
ω_{exe}	—	13.67[b]	—	12.99[e]	13.4[g]	12.9[k]
ω_{eye}	—	—	—	−0.019[e]	—	—
b state						
T_e	—	13179.5±1.1[b]	—	—	—	13195.3[k]
ω_e	—	1432.03±1.13[b]	—	—	—	1432.67[k]
ω_{exe}	—	14.18±0.283[b]	—	—	—	13.93[k]
ω_{eye}	—	−0.01±0.02[b]	—	—	—	−0.0143[k]
c state						
T_e	—	—	—	24552[e] (ν_{00})[f]	24649[g] (ν_{00})[f]	33056.87[m]
ω_e	—	—	—	—	—	796.96[m]
ω_{exe}	—	—	—	—	—	13.54[m]
ω_{eye}	—	—	—	—	—	−0.153[m]
A′ state						
T_e	—	34110[c]	—	—	34446.2[h]	34769.64[m]
ω_e	—	—	—	—	814.03[c]	814.97[m]
ω_{exe}	—	—	—	—	9.94[c]	13.29[m]
ω_{eye}	—	—	—	—	−0.566[c]	−0.183[m]
A state						
T_e	—	—	—	—	—	35399.18[m]
ω_e	—	—	—	—	—	803.92[m]
ω_{exe}	—	—	—	—	—	14.55[m]
ω_{eye}	—	—	—	—	—	−0.0651[m]
B state						
T_e	49392.8[a]	48534[d]	48311[d]	48268[a]	48543[j]	49005[n]
ω_e	752.7[a]	728.0[d]	733.7[d]	748.7[a]	757[j]	709.06[n]
ω_{exe}	16.1[a]	12.33[d]	16.18[d]	15.4[a]	14.6[j]	10.61[n]
ω_{eye}	0.0214[a]	0.261[d]	0.755[d]	0.0206[a]	—	−0.0592[n]
ω_{eze}	—	−0.0265[d]	−0.0382[d]	—	—	−0.0240[n]
ω_{eae}	—	0.0007[d]	0.0004[d]	—	—	0.00221[n]

a) Ref. 35. (without no correction for the wrong numbering of vibrational levels). b) Ref. 31. c) Ref. 15. d) Ref. 44. e) Ref. 22. f) ν_{00} represents the energy between $v' = 0$ level of c state and $v'' = 0$ level of a state. g) Ref. 16. h) Ref. 18. j) Ref. 34. k) Ref. 2. m) Ref. 11. n) Ref. 53.

molecular configuration reached by predissociation. In detail, however, some differences are found between the 193 and 248 nm excitations. One example is the c ($v' = 5$)→a emission,[17] which is weaker in the KrF excimer laser irradiation than in the ArF laser irradiation. By the 248 nm irradiation, the O_2 molecule absorbs radiation at the $v' = 9$ level of the $\Omega = 3$ component and/or $v' = 10$ of $\Omega = 1$ component of the A′ state. Thus the nascent population of the c state is considered to be smaller in the 248 nm excitation than in the 193 nm excitation. This difference in the nascent population is reflected to some extent in the stronger c→a emissions observed in the 193 nm irradiation.

2. Vibronic Relaxation Mechanism in Herzberg States. The relaxation after the nascent population may be shown as below. Considering that the level spacings are the smallest in the A′ states if the three Ω components are taken into account, it is probable that the main vibrational relaxation (cascade) among the A, A′, and c states proceeds through the manifold of the A′ state. The vibrational levels of the A state should also be involved, since strong perturbations exist be-

tween the $\Omega=2$ components of the A′ state and the A state, as discussed on the basis of absorption spectroscopy.[15] A non-negligible rapid cross relaxation (intersystem crossing) must exist between the A′ and c states in order to explain the strong A′ emission in the ArF laser irradiation. A possible mechanism is the spin-orbit coupling at higher vibrational levels of the c and A′ states. Then how does the $v'=5$ level of the c state specifically radiate? Richards and Johnson[22] explained similar unusual appearances of higher vibrational levels of the c state in Xe matrices by a more efficient supply to such levels through spin-orbit coupling from the triplet manifolds. This might also be the case for the present Ar solids; however, the more detailed discussion concerning the energy gap during the relaxation might be taken into consideration as described below. We consult the gas-phase energy levels shown in Fig. 3 by Slanger and Cosby.[11] The level energies in the gas phase can be used as good references, because the matrix effect is relatively weak for the relevant electronic states. The energy difference between one of the higher vibrational levels ($v\geq6$) of the c state and the closest lower vibrational level of the A′ state is less than several tens of cm^{-1}. This difference is increased suddenly at the $v=5$ level to 130 cm^{-1} (being estimated from the level positions shown in Fig. 3). The energy differences might differ in solids from the gas-phase values, but it is still expected that they change sharply between the levels of $v\geq6$ and that of $v=5$. This large energy difference at $v=5$ can considerably decrease the cross relaxation rate from the $v=5$ level to the closest lower level of the A′ state. The cross relaxation rate of higher vibrational levels may be much faster than the radiative decay. At the $v=5$ level, however, the cross relaxation may become so slow that the radiative decay from the c state to the $a(^1\Delta_g)$ state can make its appearance, although the main decay channel should still be the non-radiative cross relaxation. In fact, the radiative lifetime of the c state of $^{16\text{-}18}O_2$ in solids, supposed to be 1 ms,[15,18] is much longer than the present lifetime, 80 ns, of the $v'=5$ level of the c state of $^{16\text{-}16}O_2$. The reason why the emissions from lower ($v'\leq4$) vibrational levels of the c state are too weak to be detectable is not clear.

3. A′→c Population Transfer. The c→a emissions from the $v'=2,1,0$ levels of $^{16\text{-}18}O_2$ irradiated by the 193 nm irradiation in Fig. 5 deserve discussion. These emissions were already observed by Rossetti and Brus[18] by using isotopically rich O_2 molecules excited in longer wavelength regions. On the basis of the time evolution of individual levels, they tried to explain the appearance of these emissions by an accidental near coincidence between the A′ $v=0$ level and the c $v=2$ level of $^{16\text{-}18}O_2$, which is favorable for rapid cross relaxation from the A′ state to the c state, though there is another possibility for the appearance of the $^{16\text{-}18}O_2$ emissions by the 193 nm irradiation in spite of the small isotopic abundance due to possible favorable absorption of the 193 nm radiation by the $^{16\text{-}18}O_2$ molecules in the Ar solid.

4. Other Emissions from Excited O_2. The breakdown of optical selection rules in the solid environments sometimes results in strong emission from a variety of optically forbidden transitions. The $A'(^3\Delta_u)$–$X(^3\Sigma_g^-)$ transition becomes partly allowed due to the breakdown of $\Delta\Lambda=0,\pm1$ selection rule for linear molecule in the surrounding symmetry. The restrictions of changing spin are rather hard to overcome, and in fact, c→X and A′→a emissions have not been detected. There remain two emissions with no spin restriction that have not been observed: $A(^3\Sigma_u^+)\rightarrow X(^3\Sigma_g^-)$ and $c(^1\Sigma_u^-)\rightarrow b(^1\Sigma_g^+)$. Lack of the former is attributed to coupling with the A′ state resulting in the energy collecting in A′ ($v=0$) and sometimes in the c state lying lower, as has been already mentioned.

5. Emissions in Xe Solid. A relatively large different behavior is observed in Xe solid, where the emission bands have a quite different intensity distribution from those observed in other solids. The reason is, as pointed out by Richards and Johnson,[22] that they are the c–a system, involving predominantly $v'=2$ and 5. At lower temperatures, the 193 nm induced progressions can be clearly observed and assigned to the singlet c–a transition. The very strong temperature dependent quenching of the Herzberg bands[20] are taken to imply that the A and A′ triplet states of O_2 in Xe are strongly perturbed, while in Ar, Kr, and N_2, the observed molecular O_2 states are subject to only minor perturbations.

6. O Atom Production and Rare Gas–O Emissions. The production of O atoms is detected through the 193 nm photodissociation of O_2 in rare gas solids. Though the most of the dissociated O_2 molecule may recombine through the cage effect, permanent dissociation indeed occurs. Though the details are not clear, molecules at defect sites may undergo dissociation. N_2O is a more clean precursor for O atom, and most studies on the rare gas–O atom systems have been studied by using N_2O as the dopant. Calculation of the absorption and fluorescence spectra of trapped oxygen (^3P, ^1D, ^1S) in a rare gas crystal has been performed by Maillard et al.[23] The charge transfer bands of rare gas–O atoms, particularly those of Xe–O, were extensively studied by Lawrence and Apkarian.[8] Excitation of the Xe solid containing oxygen atoms between 220 and 160 nm leads to two main emissions at 3.35 and 1.65 eV, both of which arise from the same upper state. The ionic $Xe^+O^-(^1\Sigma^+)$ state is proposed as the candidate.

The migration of atomic species in rare gas solids is discussed by using molecular dynamics and simple transition-state theory.[24] Migration of atomic oxygen in Xe solids are specifically discussed by several researchers.[20,25–27]

Vibrational Relaxation of the Ground State O_2

The question arises concerning the fate of the vibrationally excited O_2 molecules. Recently, Salloum and Dubost[28] reported that the vibrational relaxation of the ground state O_2 in Ar matrices is slow; they prepared the vibrationally excited O_2 by energy transfer from the highly vibrationally excited CO. Kajihara et al.[29] have also observed the very slow vibrational relaxation in O_2-doped Ar and Kr solids under the KrF excimer laser irradiation. Thus it is expected that a relatively large amount of vibrationally excited O_2 should be

accumulated when a solid containing O_2 is repetitively irradiated by a UV laser. Kajihara et al.[30] recently succeeded in observing absorption signals from highly vibrationally excited O_2 doped in a free-standing Ar crystal irradiated by a KrF excimer laser. A free-standing crystal, different from thin-film matrices, guarantees a sufficient optical path length for estimating the concentration of vibrationally excited O_2 accumulated in the crystal.

1. B←X Absorption under Laser-Irradiation. A lot of absorption lines were observed in the UV range (180—268 nm) when the whole crystal was under irradiation by a KrF excimer laser as shown in Fig. 6.[30] Each absorption line consisted of a strong peak of a FWHM of ca. 20 cm^{-1}, being accompanied by a weak broad absorption on the higher frequency side, as illustrated in the inserted figure in Fig. 6. These features can be regarded as zero phone line and phonon wing, respectively. Most of the absorption lines could be assigned to the transitions from X state to B state. In the assignment, the molecular constants of ground state O_2 in Ar solid obtained from the b→X emission spectra[31] and the energy values of individual vibrational levels of B state in Ar solid obtained from UV absorption spectra[32—36] were consulted. However, in these previous studies,[32—36] the transitions to low vibrational levels of B state from X state were very weak; then the vibrational assignment of B state was not conclusive. Kajihara et al.[30] have confirmed that the numbering by Boursey et al.[32] is correct, on the basis of a careful reassignment procedure including the isotope shift measurements. The vibrational numbering is important in describing the potential curve in solids, and the detailed study is described in the next section.

2. Population of Vibrationally Excited O_2. The absorbance of the B←X absorption reached an almost constant value after the continuous laser irradiation for several minutes. The concentration of vibrationally excited O_2 has been estimated based on the measured absorbance and the oscillator strength values in the gas phase. The oscillator strength of the Schumann–Runge absorption bands of the gaseous O_2 are reported by Yoshino et al.[37]

The mole fraction and concentration of individual vibrational levels in the steady state obtained under a typical laser irradiation condition, using several lines to different v' levels from a common v'' level, are shown in Table 7.[30] The total concentration from v'' = 4 to 8 is 3.2×10^{16} molecules cm^{-3}, which equals 0.07% of the overall O_2. The populations of v'' larger than 8 levels could not be precisely determined due to their weak absorption. However, they are estimated to be less than 2×10^{15} molecules cm^{-3} in total.

The laser fluence dependence of the steady state concentration for each vibrational level was also studied.[30] It is found that the steady state concentration depends on the 0.9'th power of the laser fluence. A first order dependence is expected when the vibrationally excited O_2 in X state is supplied through one photon process and then decays via a certain first order process without being affected by the incident laser. Provided that the near first order dependence of the steady state concentration on the laser fluence is obeyed, a high accumulation of the vibrationally hot O_2 is expected under a stronger incident laser irradiation.

Table 7. Mole Fraction ($\alpha(v'')$) and Concentration (C) of Vibrationally Excited O_2

v''	$\alpha(v'')$	C/molecules cm^{-3}
4	$(1.8\pm0.4)\times10^{-4}$	$(8.2\pm1.8)\times10^{15}$
5	$(1.8\pm0.7)\times10^{-4}$	$(8.2\pm3.3)\times10^{15}$
6	$(1.8\pm1.0)\times10^{-4}$	$(7.9\pm4.3)\times10^{15}$
7	$(1.2\pm0.5)\times10^{-4}$	$(5.3\pm2.3)\times10^{15}$
8	$(5.7\pm2.4)\times10^{-5}$	$(2.5\pm1.1)\times10^{15}$

The values were obtained in the steady state under the KrF laser irradiation to the Ar crystal doped with 0.16% O_2 at a fluence of 4.9 mJ cm^{-2} $pulse^{-1}$ and a repetition rate of 10 Hz. ± means one standard deviation for the variation among the transition intensities to different v' levels from a common v'' level.

In the same work, absorption lines due to the transition from $a(^1\Delta_g)$ state in the UV region (200—350 nm) were also searched for, but in vain. However, this failure does not necessarily mean that the $a(^1\Delta_g)$ state can not be accumulated under certain laser irradiation conditions, because the failure may be either due to the very low $a(^1\Delta_g)$ state concentration or to the fact that the upper state reached from the $a(^1\Delta_g)$ state in the UV region is not an allowed and/or a discrete one.

3. Vibrational Relaxation Rate of Ground State O_2. The time evolution of individual v'' levels of ground state has been pursued after the interruption of the laser irradiation. Some examples are shown in Fig. 7.[29] The ordinate shows the concentration of individual vibrational levels, which has been estimated from the measured absorbance and the oscillator strength values in the gas phase, as stated before. The time evolution is not a simple exponential decay; in some levels, the population rises at first and decays. The decay rate seems to be faster with the increase of vibrational quantum number. These behaviors may indicate that the lower levels are partly supplied through the relaxation ladder from the higher vibrational levels. We have analyzed the time evolution on the basis of the two different models illustrated in Fig. 8. One is a $\Delta v=1$ (stepwise decay) model and the other is a $\Delta v=2$ (skip decay) model. The individual levels are also supplied directly from higher electronic levels such as via A′–X radiative decay. The time evolution is thus described by the equation;

$$C_n(t) = C_{n0} + k_x \int_0^t C_x(t)\mathrm{d}t - k_n \int_0^t C_n(t)\mathrm{d}t. \quad (1)$$

Here $x=n+1$ in the stepwise decay model and $x=n+2$ in the skip decay model. The analysis has been performed by using the Integrated Profile Method.[38] The most probable values for C_{n0}, k_x, and k_n have been determined so that these may result in the best fit between the estimated and experimental time evolution curves. An example of the comparison between the experimental and simulated time evolutions based on the two different models is shown in Fig. 9. It is impossible to conclude from these analyses which model is correct, though the skip model seems to give slightly bet-

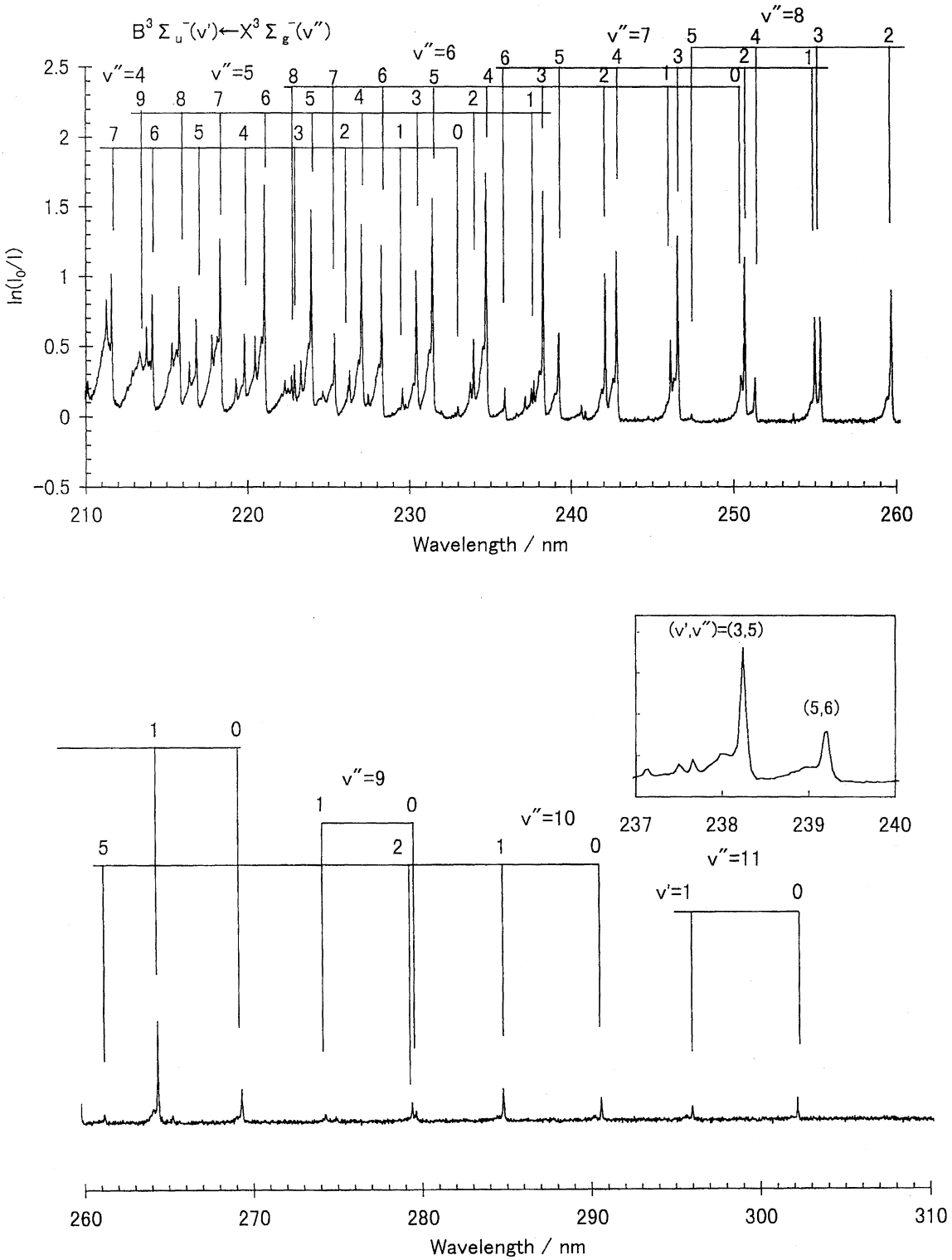

Fig. 6. Absorption spectra of 0.16% O_2-doped Ar under KrF laser irradiation. Upper, 210—260 nm, Lower, 260—310 nm. The assignment of the B(v')←X(v'') transition is shown. An enlargement of the feature of (3,5) and (5,6) lines is inserted in the lower figure. The original data are from Ref. 30.

ter coincidence between the experimental and the simulated time evolutions. The rate constants in Eq. 1 thus determined are tabulated in Table 8. Although the vibrational relaxation mechanism is not conclusively determined, it is important to notice that the decay rate is very slow, independent on the adopted relaxation model. The reasons for this very slow relaxation are, (1) the rate of phonon assisted radiationless relaxation is very slow, since the difference between the phonon energy[39] of Ar lattice (represented by the Debye frequency shown in Table 1) and the vibrational quantum of O_2 is very large; (2) radiative relaxation does not occur, since O_2 is not IR-active. The possible relaxation mechanism was also

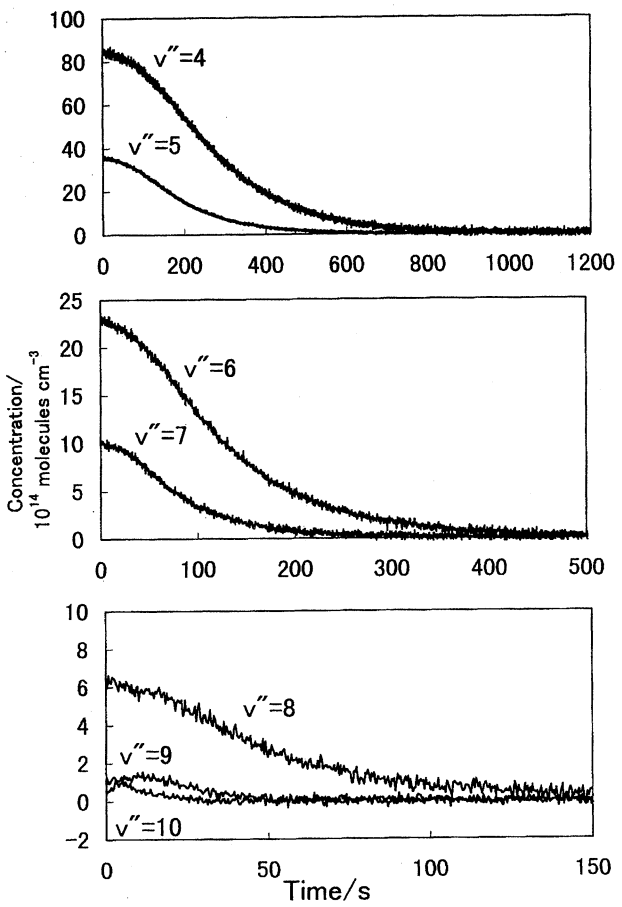

Fig. 7. Time evolution of populations of the individual vibrational levels of X state after the interruption of laser light. The O_2 (0.05%)/Ar solid has been irradiated by KrF excimer laser at 21 mJ cm^{-2}. The original data are from Ref. 29.

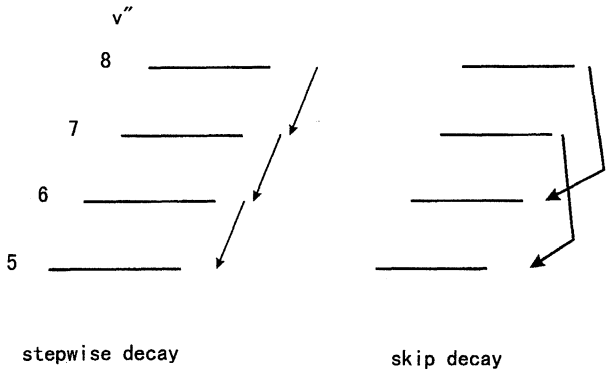

Fig. 8. The vibrational relaxation model. The "stepwise decay" model and "skip decay" model are shown.

discussed by Salloum and Dubost.[28] A theory for state-to-state vibrational multiphonon relaxation rates for a diatomic molecule in a rare gas crystal has been also proposed by Egorov and Skinner.[40]

The Total Picture of O_2 Relaxation in Ar Excited in the Neighborhood of the Dissociation Limit

1. A Picture with the a($^1\Delta_g$) State as the Energy Storage Intermediate.

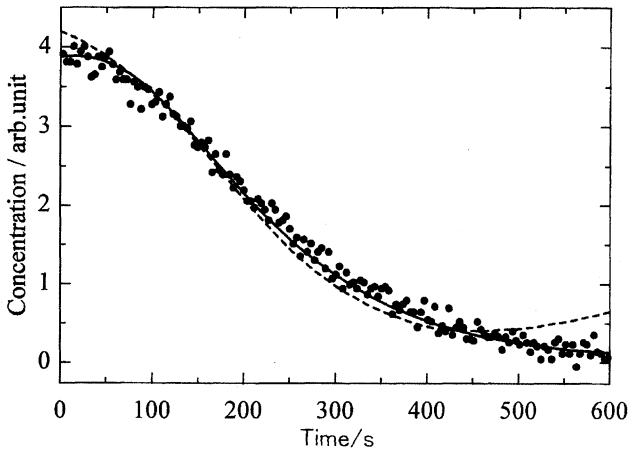

Fig. 9. Comparison between the experimental and simulated time evolutions. The time evolutions of $v'=4$ level of O_2 (0.025%)/Ar irradiation by KrF excimer laser at 21 mJ cm^{-2} are drawn. Circles are experimental data, the solid line is obtained through analysis based on the skip model, and the dashed line, the stepwise model.

Table 8. Estimated Decay Constants for Various v'' Levels of O_2(X State) Doped in Ar (0.025%) after the KrF Excimer Laser Irradiation

v''	k/s^{-1}	
	Stepwise model	Skip model
4	0.0093	0.0064
5	0.0109	0.0084
6	0.0153	0.0116
7	0.0192	0.0152
8	0.0246	0.023
9	0.0585	—

While in the red spectral range, emission from the a($^1\Delta_g$) state is not observed, the presence of the population in a($^1\Delta_g$) is verified by measurements of emission intensity vs. dark time between irradiation pulses according to Danylichev and Apkarian.[41] They showed that the A′→X emission intensity is a function of irradiation time. Several irradiation cycles at a constant laser repetition rate of 10 Hz have been checked, with different dark periods between irradiation cycles. Within a given irradiation cycle, the emission intensity is observed to decrease until a plateau is reached. The plateau level is proportional to the laser intensity. The signal decay rate is proportional to the laser power. When the laser intensity is halved, so is the decay rate and the plateau level reached. The peak intensity at the beginning of a cycle is observed to be higher when preceded by a longer dark period. The recovery rate of the peak intensity determined from a plot of peak intensity vs. dark time between irradiation cycles is 70±15 s, which is close to the radiative lifetime of a($^1\Delta_g$) state in solids (85±10 s in Ar matrices[31]). These reversible bleachings have been analyzed by using a three level model, where the ground state, as state 1; the reservoir state, which is claimed to be a($^1\Delta_g$) state judging from the recovery lifetime, as state 2; and the optically ac-

cessed upper states, as state 3. They stated that excitation of matrix isolated O_2 at 193 nm leads to efficient excitation of the molecule, whereby nearly 50% of the ground state population is transferred to the metastable singlet manifold. A kinetic analysis yields absorption cross sections of ca. 10^{-21} cm^2, from X and a($^1\Delta_g$) states. The final state from the X state has been suggested to be the repulsive wall of the A′ state where Franck–Condon factors are optimal and the oscillator strength of this transition is considered to be enhanced by mixing with the $^3\Pi_u$ state (consult Fig. 2). The final state from the a($^1\Delta_g$) state is suggested to be the repulsive $^1\Pi_u$ state, from the consideration of both the Franck–Condon principle and the conservation of spin.

2. A Picture with the Vibrationally Excited O_2 as the Energy Storage Intermediate. In the case of KrF laser irradiation, we can expect a similar picture, though the contribution of X state (vibrationally excited levels) is taken into account in place of a($^1\Delta_g$) state. The population balance analysis has been performed according to the scheme described in Fig. 10. At first, O_2 absorbs the laser light to yield Herzberg states. The excited species lose the energy gradually and relax mainly to A′ (v=0) state, from which, through the radiative transition, vibrationally excited O_2 in X state is produced, whose nascent distribution is mainly determined by the Franck–Condon factor. The vibrationally excited O_2 relaxes very slowly, and during the relaxation, laser light is successively absorbed and the B state and/or the repulsive states above the dissociation level are reached. In the cage, the excited Herzberg states are reproduced. The subsequent relaxation proceeds as before.

The detailed procedure of the population balance analysis is the following, where the contribution of a($^1\Delta_g$) state is neglected and the skip model for the vibrational relaxation is adopted.

The population balance equation of any v'' level under steady state condition, ss, is equated as

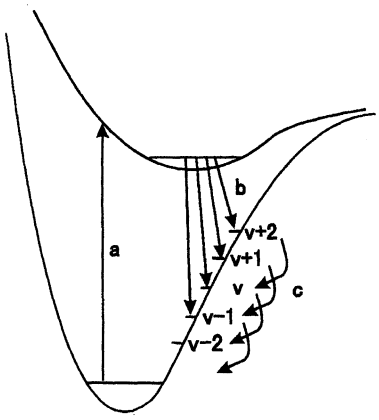

Fig. 10. A schematic model of relaxation process of O_2 excited by KrF excimer laser irradiation. (a) is the absorption to Herzberg states, which is followed by vibronic relaxation to A′ (v=0) level, from which the radiative decay (b) proceeds. The vibrational levels of X state relax (c) according to a certain decay mechanism. Here is shown the skip decay model.

$$\sigma I N Q_{v''} + k_{v''+2}[O_{2,v''+2}]_{ss} - k_{v''}[O_{2,v''}]_{ss} = 0, \quad (2)$$

where σ (in cm^2) is the absorption cross section of the laser irradiation at 248 nm, I, the intensity of laser light (in photon $cm^{-2}\,s^{-1}$), N, the total O_2 density (in molecules cm^{-3}), $Q_{v''}$, the fraction to the v'' level during the A′→X transition which is estimated from the Franck–Condon factor, $k_{v''}$, the vibrational decay rate constant of the v'' level, and $[O_{2,v''}]_{ss}$, the steady state concentration of the v'' level. The estimated σ value should be independent of v'' if the above simple model is completely obeyed. Eventually it has been poorly obeyed, which indicates that the model is too simple. However, the order of σ of 10^{-22} cm^2 obtained from the above estimation is in agreement with the value of 4×10^{-22} cm^2 obtained through extrapolation of the absorbance augmentation relationship obtained by Oshima et al.[7] in dense gases with using the solid molecular density as the equivalent gas density required in the above estimation.

The relative contribution of a($^1\Delta_g$) and X state as the intermediate state, which should be wavelength dependent, can not be determined in either the 193 nm[41] or the 248 nm[30] irradiation cases. It is desirable to pursue more quantitative analysis further.

B State Potential Curves and Cage Effect

1. Vibrational Analysis of B State Levels. Compared with an abundance of information of B state in the gas phase, only a few reports exist on the spectroscopic properties of the B state in solids. Pure solid O_2 at low temperatures shows only a continuum in the B–X absorption region.[42] Under matrix isolation conditions, Schumann–Runge bands were observed by Bass and Broida.[33] Schnepp and Dressler[34] reported, for the first time, modified potential curves of the B state in Ar and N_2 matrices. Subsequently, Boursey, Roncin and Damany (BRD)[32] reported the B–X bands of O_2 in Ne, Ar, Kr, and Xe matrices and reassigned the vibrational progression observed in Ar matrices to v' values lower by one from the assignment of Schnepp and Dressler.[34] Later, Fugol et al.[35] claimed to have confirmed the assignment of BRD for O_2 in Ar matrices. This numbering is accepted by later researchers. Bahrdt and Schwentner[43] published the excitation spectrum of the B–X transition in Ar matrices by monitoring the emission due to the A′–X transition. Very recently, Salloum and Dubost[28] measured the B–X excitation spectra in the UV-vis region by elegantly generating vibrationally excited O_2 in the X state through energy transfer from CO to O_2 in Ar and Kr matrices. The numbering by Fugol has been also adopted by these researchers. However, the absorption to low vibrational levels of B state could not be observed due to the unfavorable Franck–Condon factors, or even they were observed, they suffered from broad phonon wings. Then the numbering and energy values of vibrational levels of B state from the absorption measurements have not been considered conclusive.

As shown in the previous section, vibrationally excited O_2 in X state is accumulated under the KrF excimer laser irradiation in O_2-doped Ar or Kr solids. Since the tran-

sitions from the high vibrational levels in X state to the low vibrational levels in B state are almost vertical, the absorption lines are strong and sharp. The energy values are much more precisely determined than those by previous researchers. Kajihara and Koda[30,44] performed measurement of the isotope shift between $^{16}O_2$ and $^{18}O_2$ for the sake of reliable vibrational numbering. The determined numbering was also made certain by comparing the observed intensity distribution with calculated Franck–Condon factors. In conclusion, the vibrational numbering of the B state was raised by one from the now-accepted one,[35] and thus the original numbering by Schnepp and Dressler[34] has been recovered.

2. B State Potential Curve. The vibrational levels up to the values over the gas phase dissociation limit to $O(^3P)+O(^1D)$ are observed by Gudipati[36] in Ar and Kr matrices using Syncrotron radiation facility (BESSY). Based on the vibrational energies for intermediate vibrational levels from the absorption by vibrationally excited O_2 ($v'=0$—8 in Ar, and $v'=0$—10 in Kr) and values for higher vibrational values from VUV absorption measurements, the potential curves of B state has been estimated,[44] employing Oldenberg's method.[45]

In order to employ this method, the potential curve to the left of the minimum (to shorter interatomic distance, r, than the equilibrium interatomic distance, r_e) must be known. In the present case the gas-phase potential curve[46] of O_2 is assumed to apply to the molecule in the crystal for the left of the minimum, since in this region the environment would not make itself felt. Oldenberg made use of the basic relation:

$$\oint p\mathrm{d}q = 2\int_{r_{\min}}^{r_{\max}} [2\mu(E-V)]^{1/2}\mathrm{d}r = (v'+1/2)h. \qquad (3)$$

Here μ is the reduced mass of the molecule, E is the energy of the state v', and V is the potential energy which is a function of r. The limits of the integration, $r_{\min}$ and $r_{\max}$, are the two values of r for which $V(r)$ has the value E, and, as already mentioned, $r_{\min}$ is assumed to be known. The upper limit $r_{\max}$ is adjusted by a trial and error method until the area under the curve satisfies Eq. 3. The energies obtained by Kajihara et al.[30] were adopted for the lower vibronic levels ($v'\leqq 8$ in Ar and $v'\leqq 10$ in Kr) and those obtained by Gudipati[36] were employed for the higher vibronic levels ($9\leqq v'\leqq 15$ in Ar and $11\leqq v'\leqq 15$ in Kr) after raising v' values by one. Vibrational spacings were smoothed by fitting them to a fifth order polynomial in $(v'+1/2)$ and the smoothed values of the energies were adopted for the computation of the potential curve. In Fig. 11 the computed potential curves for O_2 in Ar and Kr crystals are drawn. For comparison, the potential curve for the gas-phase O_2[46] is also given. The $v'=0$ level of X state was adopted as the energy origin both for the gas-phase and solid potential, considering that X state is much less affected by the environment than the B state.

It is clear that the B state potential curves for the doped O_2 in rare-gas solids are steeper than that of the gas-phase molecule. It is seen from Fig. 11 that these potential curves begin to deviate from that of the gas-phase molecule near $v'=3$ for $^{16}O_2$, which corresponds to $r_{\max}$ of 0.18 nm. The

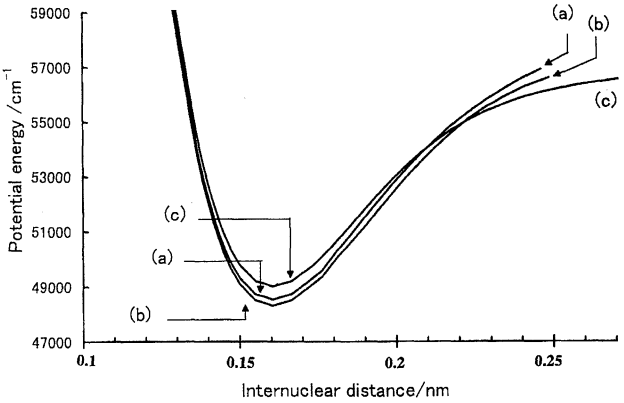

Fig. 11. The potential curves of O_2 in $B(^3\Sigma_u^-)$ state in Ar (a) and Kr (b) solids. The potential curve for O_2 in the gas phase (c) is also given. The origin of the energy (cm^{-1}) is the $v''=0$ level of X state, common for the gas and solids. The original data are from Ref. 44.

potential curves in the rare gas solids are still considerably steep in the energy region higher than the dissociation energy of the gas-phase O_2 and some vibrational levels exist in this region. They are found to be stabilized by 471 in Ar and 694 cm^{-1} in Kr solid. The stabilization can be ascribed to the effect of abstracting force between the expanded electron orbitals of B state and the electron orbitals of host atoms. The A′ state of O_2 in rare gas solids is stabilized much less than that of the present B state, as tabulated in Table 6. The extent of stabilization seems to be determined by the properties of electronic state of O_2 and of host atoms.

Concluding Remarks

The energy levels, potentials and relaxation mechanism of O_2 doped in rare gas solids have been made clearer in these years. The efficient cross-relaxation among nested Herzberg states, specific energy transfer dependence on the energy gap between relevant levels, and very slow vibrational relaxation in the ground state seem to be inherent in the O_2 molecule doped in low temperature rare gas and N_2 solids.

However, more fundamental understanding of the above findings are desirable, through both experimental and theoretical efforts. More precise theoretical potential curves of O_2 doped in rare gas solids and the corresponding wave packet analysis, together with femto-second spectroscopic measurements of the dissociation process, if possible, would be very helpful in the near future.

References

1) G. Herzberg, *Can. J. Phys.*, **31**, 657 (1953).
2) P. H. Krupenie, *J. Phys. Chem. Ref. Data*, **1**, 423 (1972).
3) T. G. Slanger, *J. Chem. Phys.*, **69**, 4779 (1978).
4) P. C. Wright, *Chem. Phys. Lett.*, **71**, 127 (1980).
5) B. Coquart and D. A. Ramsay, *Can. J. Phys.*, **64**, 36 (1986).
6) T. G. Slanger, D. L. Huestis, P. C. Cosby, H. Naua, and G. Meijer, *J. Chem. Phys.*, **105**, 9393 (1996).
7) Y. Oshima, Y. Okamoto, and S. Koda, *J. Phys. Chem.*, **99**, 11830 (1995).

8) W. G. Lawrence and V. A. Apkarian, *J. Chem. Phys.*, **97**, 2229 (1992).
9) N. Schwentner, O. Doesssel, and H. Nahme, *AIP Conf. Proc.*, **90**, 584 (1970).
10) W. Rudnick, R. Haensel, H. Nahme, and N. Schwentner, *Phys. Status Solidi A*, **87**, 319 (1985).
11) T. G. Slanger and P. C. Cosby, *J. Phys. Chem.*, **92**, 267 (1988).
12) R. N. Zare, A. L. Schmeltekopf, W. J. Harrop, and D. L. Albritton, *J. Mol. Spectrosc.*, **46**, 37 (1973).
13) A. V. Danylichev, V. E. Bondebey, V. A. Apkarian, S. Tanaka, H. Kajihara, and S. Koda, *J. Chem. Phys.*, **103**, 4292 (1995).
14) S. S-L. Chiu, A. S-C. Cheung, M. Finch, M. J. Jamieson, K. Yoshino, A. Dalgarno, and W. H. Parkinson, *J. Chem. Phys.*, **97**, 1787 (1992).
15) J. Goodman and L. E. Brus, *J. Chem. Phys.*, **67**, 1482 (1977).
16) H. Kajihara, T. Okamura, F. Okada, and S. Koda, *Laser Chem.*, **15**, 83 (1995).
17) F. Okada, H. Kajihara, and S. Koda, *Chem. Phys. Lett.*, **192**, 357 (1992).
18) R. Rossetti and L. E. Brus, *J. Chem. Phys.*, **71**, 3963 (1979).
19) R. L. Brooks, *J. Chem. Phys.*, **85**, 1247 (1986).
20) A. V. Danylichev and V. A. Apkarian, *J. Chem. Phys.*, **99**, 8617 (1993).
21) A. S.-C. Chueng, K. Yoshino, J. R. Esmond, S. S.-L. Chiu, D. E. Freeman, and W. H. Parkinson, *J. Chem. Phys.*, **92**, 842 (1990).
22) J. L. Richards and P. M. Johnson, *J. Chem. Phys.*, **65**, 3948 (1976).
23) D. Maillard, J. Fournier, H. M. Mohammed, and C. Girardet, *J. Chem. Phys.*, **78**, 5480 (1983).
24) Y. Guo and D. L. Thompson, *J. Chem. Phys.*, **103**, 9024 (1995).
25) H. Kruger and E. Weitz, *J. Chem. Phys.*, **96**, 2846 (1992).
26) W. G. Lawrence and V. A. Apkarian, *J. Chem. Phys.*, **97**, 6199 (1992).
27) A. V. Danilychev and V. A. Apkarian, *J. Chem. Phys.*, **100**, 5556 (1994).
28) A. Salloum and H. Dubost, *Chem. Phys.*, **189**, 179 (1994).
29) H. Kajihara, T. Okamura, and S. Koda, in "Structures and Dynamics of Clusters," ed by T. Kondow, K. Kaya, and A. Terasaki, Universal Academy Press, Inc., Tokyo (1995), p. 409.
30) H. Kajihara, T. Okamura, and S. Koda, *Chem. Phys. Lett.*, **256**, 126 (1996).
31) A. C. Becker, U. Schurath, H. Dubost, and J. P. Galaup, *Chem. Phys.*, **125**, 321 (1988).
32) E. Boursey, J. Roncin, and N. Damany, *Chem. Phys. Lett.*, **5**, 584 (1970).
33) A. M. Bass and H. P. Broida, *J. Mol. Spectrosc.*, **12**, 221 (1964).
34) O. Schnepp and K. Dressler, *J. Chem. Phys.*, **42**, 2482 (1965).
35) I. Ya. Fugol, L. G. Gimpelevich, and L. I. Timchenko, *Opt. Spectrosc.*, **40**, 159 (1976).
36) M. S. Gudipati, *Chem. Phys.*, **201**, 451 (1995).
37) K. Yoshino, D. E. Freeman, J. R. Esmond, and W. H. Parkinson, *Planet. Space Sci.*, **31**, 339 (1983).
38) K. Yamasaki, *Bull. Chem. Soc. Jpn.*, **70**, 89 (1997).
39) H. J. Jodl, in "Chemistry and Physics of Matrix Isolated Species," ed by L. Andrews and M. Moscovits, Elsevier, Amsterdam (1989), p. 343.
40) S. A. Egorov and J. L. Skinner, *J. Chem. Phys.*, **106**, 1034 (1997).
41) A. V. Danilychev and V. A. Apkarian, *Chem. Phys. Lett.*, **246**, 139 (1995).
42) J. Romand and J. G.-Mayence, *J. Phys. Radium*, **15**, 62 (1954).
43) J. Bahrdt and N. Schwentner, *J. Chem. Phys.*, **85**, 6229 (1986).
44) H. Kajihara and S. Koda, *J. Mol. Spectrosc.*, in press.
45) O. Oldenberg, *Z. Phys.*, **56**, 563 (1929).
46) A. S-C. Cheung, D. K-W. Mok, Yan Sun, and D. E. Freeman, *J. Mol. Spectrosc.*, **163**, 9 (1994).
47) D. Kunszner and N. Schwentner, *J. Chem. Phys.*, **98**, 6965 (1993).
48) W. G. Lawrence and V. A. Apkarian, *J. Chem. Phys.*, **97**, 2224 (1992).
49) H. Kajihara, F. Okada, and S. Koda, *Chem. Phys.*, **186**, 395 (1994).
50) S. Tanaka, H. Kajihara, S. Koda, and V. A. Apkarian, *Chem. Phys. Lett.*, **233**, 555 (1995).
51) L. J. Shoen and H. P. Broida, *J. Chem. Phys.*, **32**, 1184 (1960).
52) J. P. Galaup, R. Charneau, and H. Dubost, *J. Lumin.*, **40/41**, 250 (1988).
53) C. O. Laux and C. H. Kruger, *J. Quant. Spectrosc. Radiat. Transfer*, **48**, 9 (1992).

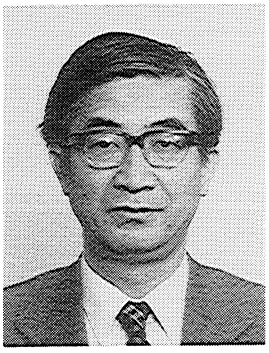

Graduated from the University of Tokyo in 1965. Ph. D from the University of Tokyo (Industrial Chemistry) in 1970. NRC fellow at National Research Council of Canada, Ottawa, 1972—1974. Lecturer, 1980—1981, Associate Professor, 1981—1990, and Professor of the University of Tokyo, 1990—present. His research fields are reaction chemistry, laser chemistry, and chemical reaction engineering. At present, he is interested in cryogenic photophysics and chemistry, heterogeneous reactions related to atmospheric chemistry, and reaction mechanism and applications of supercritical fluids reactions.

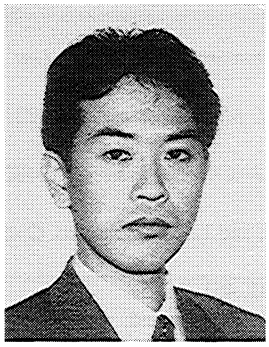

Graduated from the University of Tokyo in 1991. Ph. D from the University of Tokyo (Chemical System Engineering) in 1996. Post-doctoral at Yokohama National University since 1997. At present, his research interests range from cryogenic photochemistry to risk-assessments concerned with environmental pollutants.